Adaptive phase-distortion correction based on parallel gradient-descent optimization

M. A. Vorontsov and G. W. Carhart

New Mexico State University, Las Cruces, New Mexico 88003, and Army Research Laboratory, Adelphi, Maryland 20823

J. C. Ricklin

Army Research Laboratory, Adelphi, Maryland 20823

Received January 14, 1997

We describe an adaptive wave-front control technique based on a parallel stochastic perturbation method that can be applied to a general class of adaptive-optical system. The efficiency of this approach is analyzed numerically and experimentally by use of a white-light adaptive-imaging system with an extended source. To create and compensate for static phase distortions, we use 127-element liquid-crystal phase modulators. Results demonstrate that adaptive wave-front correction by a parallel-perturbation technique can significantly improve image quality. © 1997 Optical Society of America

Adaptive correction of phase-distorted extended source images is perhaps the most well known but yet intriguing problem in adaptive optics. Formally, for extended-source adaptive imaging an approach based on gradient-descent optimization of an image-quality metric $J = J(u_1, \ldots, u_j, \ldots, u_N)$, where u_j, $j = 1, \ldots, N$, are wave-front shape-control parameters, can be applied.[1–3] For measuring gradient components, the conventional sequential-perturbation technique is commonly used. This procedure is based on estimation of the true gradient by application of small perturbations δu_j one at a time and measurement of the corresponding changes δJ_j in an image-quality metric. The ratios $\delta J_j/\delta u_j$ are used as approximations to the true gradient components.[4] Complete knowledge of the true gradient requires N sequential perturbations, with time losses that increase as the number of control channels N increases. A similar problem is faced when one uses the multidither technique.[5] The processing time for large N is the main drawback for both simple sequential perturbation and the multidither gradient-descent techniques, resulting in significant limitation to the potential resolution of adaptive-optical systems.

Here we suggest an alternative technique that provides multichannel parallel signal processing for adaptive wave-front control. This method is based on the stochastic parallel gradient-descent algorithm recently developed for model-free supervised learning in artificial neural networks.[6,7] Consider an adaptive-imaging system with N control channels (Fig. 1). This system includes an image-quality analyzer that can either measure or calculate an image-quality metric $J = J(u_1, \ldots, u_j, \ldots, u_N)$. Assume that small random perturbations δu_j of the control signals u_j are simultaneously applied to all N wave-front control channels. The perturbation components δu_j have fixed amplitudes, i.e., $|\delta u_j| = \delta u$, and random signs with equal probabilities for $\delta u_j = \delta u$ and $\delta u_j = -\delta u$. Define perturbation of J as $\delta J = J(u_1 + \delta u_1, \ldots, u_j + \delta u_j, \ldots, u_N + \delta u_N) - J(u_1, \ldots, u_j, \ldots, u_N)$ and the stochastic approximation to the true gradient component $\partial J/\partial u_j$ by the ratio $\delta J/\delta u_j$.[6,7]

For image-quality-metric optimization, conventional gradient procedures can be applied, the only difference being that instead of the true gradient the stochastic approximation is used. For the simplest gradient-descent algorithm we have

$$u_j^{(n+1)} = u_j^{(n)} - \gamma(\delta J/\delta u_j), \tag{1}$$

where n is the gradient-descent iteration number and γ is a weight coefficient.

The efficiency and performance of the parallel gradient-descent algorithm [Eq. (1)] were analyzed through numerical simulation of an incoherent adaptive-imaging system with a random aberration $W(\mathbf{r})$ located in the exit pupil. We used a wave-front-corrector model with a square array of $N = m \times m$ elements with piston-only-type response functions $S_j(\mathbf{r})$ [$S_j(\mathbf{r}) = 1$ inside any element and zero otherwise]. The random aberrations $W(\mathbf{r})$ had a similar representation. Phase-distortion amplitudes were taken as δ-correlated random variables with a uniform probability distribution within the interval $\pm\pi$. To characterize the aberration level, we used a standard deviation σ_W of $W(\mathbf{r})$.

We performed calculations on a 128×128 uniform-square grid, using a standard approach based on the optical transfer function for an incoherent imaging system with aberrations.[8] For parallel gradient-descent optimization the image-quality metric

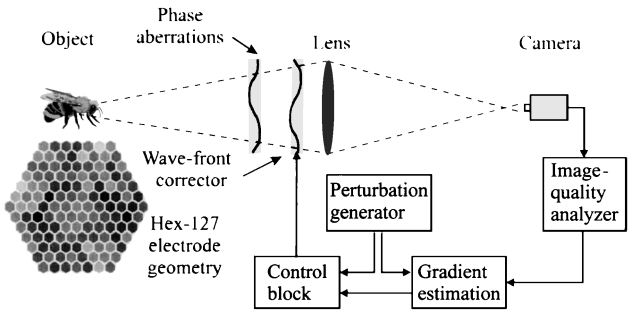

Fig. 1. General schematic for the adaptive-imaging system; the wave-front-corrector electrode geometry used in the experiment is at the bottom left.

0146-9592/97/120907-03$10.00/0

$$J = J^{\mathrm{ph}} = \int |F\{\exp[i\alpha I(\mathbf{r})]\}|^4 \mathrm{d}^2\mathbf{q} \qquad (2)$$

introduced in Ref. 3 was used. Here $I(\mathbf{r})$ is a normalized image-plane intensity distribution, α is a parameter, and $F\{*\}$ is the Fourier-transform operator.

Results of adaptation by use of the parallel-perturbation algorithm [Eq. (1)] for a system with $N = 64, 256, 1024$ control channels are shown in Figs. 2 and 3. For $N = 64$ and $N = 256$ we used the random phase screen shown in Fig. 3a, and for $N = 1024$ the phase screen shown in Fig. 3b was used. Distorted and corrected images, respectively, are shown in Figs. 2a and Fig. 2d ($N = 256$) and in Figs. 3e and Fig. 3f ($N = 1024$). Corresponding residual phase maps are presented in Figs. 3c and Fig. 3d. The original undistorted image is given in Fig. 2e. The evolution curve corresponding to the conventional gradient technique is shown by the dashed curve ($N = 64$) in Fig. 2. Convergence for the conventional technique occurred with a factor-of-3 fewer iterative steps. However, one step of phase update required N perturbations for this technique but only one perturbation for the stochastic gradient-descent algorithm. In our calculations convergence of the parallel gradient-descent algorithm required approximately $N/3$ less computational time than the conventional gradient-descent technique. Several conclusions can be made based on these calculations: (a) For every case that we observed convergence of the iterative process led to significant image-quality improvement. Speed of convergence was dependent on the control-channel number N and decreased noticeably when N was increased. (b) Except for phase distortions with relatively small amplitudes ($\sigma_W < 0.2\pi$), residual phase was not uniform and contained local regions with approximately equal phase values (see Figs. 3c and 3d). Phase differences in most regions were $\sim 2\pi$. Note that for the wave-front corrector with piston-only-type elements that was used here the observed 2π phase shift does not affect adaptive-system performance but rather indicates nonuniqueness of the solution.[1] (c) Depending on the initial conditions for the control parameters u_j, we often obtained different stationary-state phase distributions. Nevertheless, values obtained for the image-quality metric were close to one another and remained within a small vicinity ϵ of the absolute minimal value J^{ph} that corresponded to the undistorted image. These results indicate the existence of a number of image-quality-metric local minima—a typical hazard for adaptive systems based on gradient-descent optimization. Similar to the conventional technique, the stochastic parallel gradient-descent algorithm cannot guarantee optimal wave-front correction but does offer a significant reduction in the time required for adaptation-process convergence.

For experimental analysis of the parallel gradient-descent technique we used the adaptive-imaging system shown in Fig. 1. This system included two liquid-crystal (LC) Hex-127 spatial phase modulators from Meadowlark Optics, one to create random phase distortions and the second to compensate for their influence. Each phase modulator contains 127 individually addressed hexagonal LC cells, each with an active area 14.7 mm in diameter. The phase-modulation amplitude is $\sim 2.8\pi$ (for $\lambda = 0.514$ μm), and the characteristic response time is ~ 0.2 s. The LC modulators were placed in the pupil plane of the imaging lens, which had a focal length of 35 cm. As an object we used an optical fiber bundle cross section 2 mm in diameter containing individual fibers with diameters of ~ 50 μm. The other end of the optical fiber bundle was illuminated by white light. A polarizer aligned with the LC modulators' optical axes was placed in front of the first phase modulator.

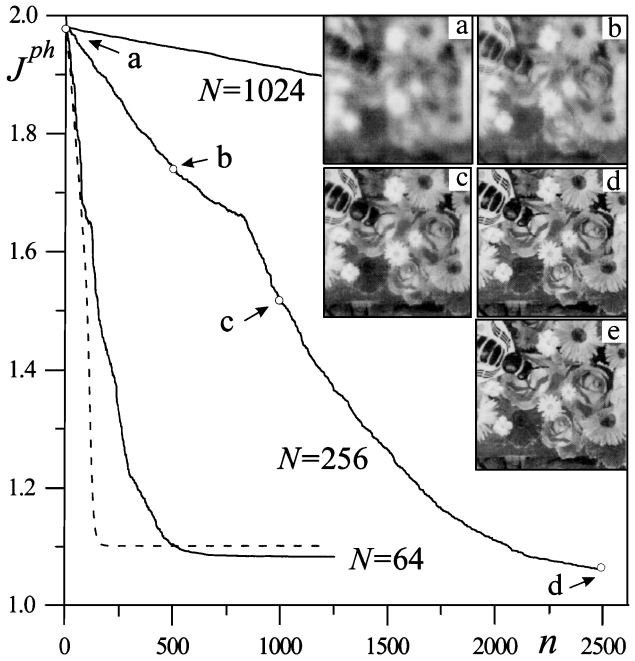

Fig. 2. Evolution curves J^{ph} versus iterations n for three numbers of control channels N: a–d correspond to marked points on the evolution curve for $N = 256$. The algorithm parameters are $\delta u = 0.004$, $\gamma = 4.0 \times 10^{-5}$, and $\alpha = 1$. An undistorted image corresponds to the point $J^{\mathrm{ph}} = 1.0$. The dashed curve corresponds to conventional gradient-descent optimization.

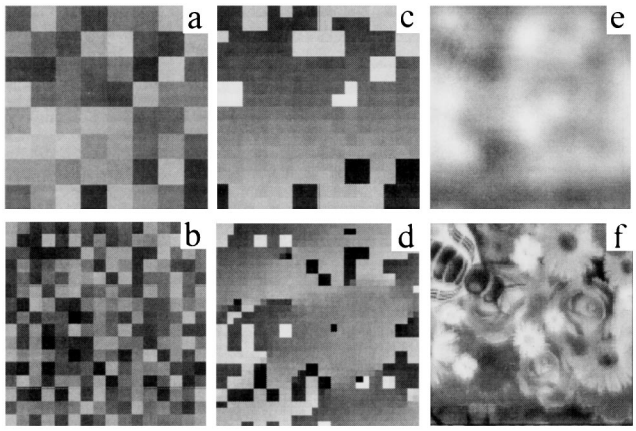

Fig. 3. Introduced (a, b) and residual (c, d) phase distortions in a gray-scale representation of amplitude 2π. Distorted (e) and corrected (f) images resulted from phase maps b and d, respectively. Image f corresponds to $n = 10,000$ iterations. Phase-screen parameters are a, $\sigma_W = 0.56\pi$, and b, $\sigma_W = 0.56\pi$.

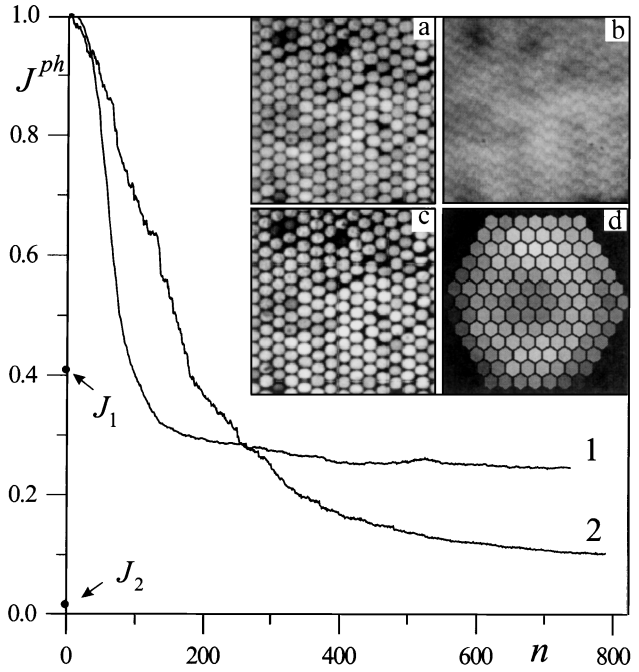

Fig. 4. Correction of a phase-distorted image with Eq. (3): phase-distortion standard deviation $\sigma_W = 0.4\pi$, $\alpha = 1$ (curve 1), and $\alpha = 3$ (curve 2). Curve 1, system with a single LC phase modulator, with a, undistorted, b, distorted, and c, corrected images. Corrected image c, obtained after $n = 750$ iterations, corresponds to phase map d of amplitude 0.4π. Curve 2, system with two LC phase modulators.

Phase aberrations in the imaging system were created with a PC computer connected to the first LC modulator. The adaptive system's feedback loop included a CCD camera connected to an image processor in the computer and to the second LC phase modulator. The computer calculated the image-quality metric, generated the stochastic perturbations, and calculated the control voltages that were then applied to the correcting LC phase modulator. Updating the control voltage required ~0.8 s.

For wave control we used a modified version of the algorithm in Eq. (1). To produce a smooth phase shape, we introduced into Eq. (1) additional connections between the N_{nb} closest neighboring elements,

$$u_j^{(n+1)} = (1-\beta)u_j^{(n)} + \frac{\beta}{N_{nb}}\sum_{l=1}^{N_{nb}} u_l^{(n)} - \gamma\frac{\delta J}{\delta u_j} - \left[\frac{1}{N}\sum_{l=1}^{N} u_l^{(n)} - u_0\right], \quad (3)$$

that are accounted for in the second term on the right-hand side of Eq. (3). The numbers N_{nb} are different for control elements located in the middle region ($N_{nb} = 6$) and along the wave-front-corrector aperture boundary ($N_{nb} = 4$). Coefficient β characterizes the strength of interconnections and in most cases was within the range $0 < \beta < 0.01$. The last term in Eq. (3) was introduced to prevent possible drift of the aperture-averaged phase-mean value during the adaptation process. Point u_0 corresponds to the middle of the LC phase-modulator dynamic range.

Consider first the results obtained when the imaging system had only one LC phase modulator (self-compensation). We introduced phase distortions by applying random voltages to all 127 electrodes of the LC phase modulator. The adaptation evolution curve along with the undistorted, the distorted, and the corrected images is shown in Fig. 4. The image-quality metric value $J^{\mathrm{ph}} = J_1$ in Fig. 4 corresponds to the absence of phase distortions. Notice that the image-quality metric actually achieved was less than the image-quality metric value J_1 (see curve 1 in Fig. 4). This indicates the adaptive system compensated not only for the phase distortions that were introduced but also for the aberrations from the imaging and the CCD camera lenses. The improvement in image quality is noticeable when one compares the undistorted and the corrected images in Fig. 4.

We also investigated performance of the imaging system when it was operated with two LC phase modulators. Random voltages were applied to one of the LC phase-modulator electrodes, causing phase distortions of amplitude 2π. The corresponding adaptation-process evolution curve is shown in Fig. 4 (curve 2). The value of image-quality metric J_2 in Fig. 4, corresponding to the undistorted image, was not achieved; nevertheless, the adaptive system significantly improved the quality of the original distorted image.

The primary advantage of the approach for adaptive wave-front correction presented here is the parallel nature of the algorithm that can be implemented with analog very large scale integration hardware.[7] A combination of analog very large scale integration chips implementing parallel stochastic perturbation algorithms and high-resolution fast LC phase modulators can provide inexpensive and effective adaptive-optical systems.

We thank Kelvin Wagner, who brought to our attention the stochastic error-descent algorithms, and Gert Cauwenberghs for helpful discussions. Experiments were performed at the Army Research Laboratory's Intelligent Optics Lab.

References

1. R. K. Tyson, *Principles of Adaptive Optics* (Academic, San Diego, Calif., 1991).
2. A. Buffington, F. S. Crawford, R. A. Muller, A. J. Schwemin, and R. G. Smits, J. Opt. Soc. Am. **67,** 298 (1977).
3. M. A. Vorontsov, G. W. Carhart, D. V. Pruidze, J. C. Ricklin, and D. G. Voelz, J. Opt. Soc. Am. A **13,** 1456 (1996).
4. M. A. Vorontsov, G. W. Carhart, D. V. Pruidze, J. C. Ricklin, and D. G. Voelz, Appl. Opt. **36,** 3319 (1997).
5. T. R. O'Meara, J. Opt. Soc. Am. **67,** 315 (1977).
6. A. Dembo and T. Kailath, IEEE Trans. Neural Networks **1,** 58 (1990).
7. G. Cauwenberghs, J. Analog Integ. Circ. Signal Process. **1,** 14 (1996).
8. J. W. Goodman, *Introduction to Fourier Optics* (McGraw-Hill, San Francisco, Calif., 1968).